Measurement of the reflection–polarization pattern of the flat water surface under a clear sky at sunset

József Gál[a], Gábor Horváth[a,*], Viktor Benno Meyer-Rochow[b,1]

[a]*Department of Biological Physics, Eötvös University, Pázmány sétány 1, H-1117 Budapest, Hungary*
[b]*Department of Biology (Zoology), University of Oulu, Linnanmaa A, SF-90401 Oulu, Finland*

Dedicated to Prof. Dr. Rudolf Schwind (Institut für Zoologie, Universität Regensburg, Germany) the expert on the polarization of water-surface-reflected light and its biological function, and to Prof. Dr. Rüdiger Wehner (Zoologisches Institut, Universität Zürich, Switzerland) on the occasion of his 60th birthday.

Abstract

Using 180° field of view imaging polarimetry, we measured the polarization characteristics (degree and angle of linear polarization) of the entire clear sunset sky and the reflection–polarization pattern of the flat water surface under this sky in order to test the validity of the earlier theoretical predictions made by Horváth, G. (1995) [Reflection–polarization patterns at flat water surfaces and their relevance for insect polarization vision. *Journal of Theoretical Biology, 175,* 27– 37] and Schwind, R., & Horváth, G. (1993) [Reflection–polarization pattern at water surfaces and correction of a common representation of the polarization pattern of the sky. *Naturwissenschaften, 80,* 82–83] on the fine structure of this reflection–polarization pattern. We compared the measured reflection–polarization pattern with the theoretical reflection–polarization patterns computed for single-scattering Rayleigh skylight and measured real skylight reflected from the flat water surface, the repolarization characteristics of which are described by the Fresnel theory. Analysing and comparing the theoretical and measured reflection–polarization patterns, we could establish that the earlier predictions of Horváth (1995) and Schwind and Horváth (1993) were correct. Contrary to other full-sky polarimeters, our 180° field of view rotating-analyzer imaging photopolarimeter is useful not only for sky measurements, but also for downward viewing polarimetry. It can be used in atmospheric optics as well as in biological investigations involving animal polarization vision and orientation on the basis of skylight polarization or water-surface-reflected polarized light. © 2001 Elsevier Science Inc. All rights reserved.

Keywords: Celestial polarization; Reflection polarization of skylight; Air–water interface; Twilight; Sunset sky; Fresnel reflection; 180° Field of view imaging polarimetry

1. Introduction

The clear sky has a characteristic polarization pattern (Coulson, 1988; Horváth & Wehner, 1999; Können, 1985). If the partially linearly polarized skylight is reflected from the water surface, its polarization state (degree and angle of polarization) changes, because the amplitude reflection coefficients of the air–water interface for horizontal and vertical polarization of incident light differ slightly from each other. The repolarization of the water-surface-reflected skylight can be calculated on the basis of the Fresnel

formulae (Mueller calculus; Guenther, 1990). Due to this repolarization of the reflected skylight, the flat water surface possesses a reflection–polarization pattern quite different from that of celestial polarization.

Although the polarization of water-surface-reflected skylight is a striking optical phenomenon in the natural environment, 180° field of view reflection–polarization patterns of the water surface have never been measured before. On the one hand, it is difficult to measure these patterns over natural water surfaces because of the almost ever present surface disturbances in the form of ripples. On the other hand, for theoretical calculations of the reflection polarization of skylight at the air–water interface the water surface should be as smooth as possible. Nevertheless, a number of authors have computed the statistical distributions for reflection patterns from rough optical surfaces. While most

* Corresponding author. Tel.: +36-1-372-2765; fax: +36-1-372-2757.
E-mail addresses: gh@arago.elte.hu (G. Horváth), vmr@cc.oulu.fi (V.B. Meyer-Rochow).
[1] Tel.: +358-8-553-1237; fax: +358-8-537-6203.

treatments have been for intensity only (e.g., Mobley, 1994), there has been recent interest in the statistical distribution of polarimetric reflection from stationary and nonstationary rough surfaces (Shaw, 1999).

Using the Fresnel formulae and assuming a theoretical polarization pattern of the sky calculated on the basis of the single-scattering Rayleigh model, Horváth (1995) and Schwind and Horváth (1993) calculated the polarization pattern of Rayleigh skylight reflected from the flat water surface. Using videopolarimetry, Horváth and Varjú (1997) measured the reflection–polarization characteristics of different water bodies. These patterns are relevant for the polarization vision of insects associated with water, because these insects detect their aquatic habitat on the basis of the horizontally polarized water-surface-reflected light (Schwind, 1995). From the theoretical calculations, it is clear that the fine structure of the reflection–polarization pattern of the water surface depends on the zenith distance of the sun and is the most complex and interesting under a clear sky at sunset. Till now it had not been possible to test experimentally the theoretical predictions of Horváth (1995) and Schwind and Horváth (1993) on the fine structure of the reflection–polarization pattern of a flat water surface.

In this work we report how 180° field of view imaging polarimetry allowed us to measure the reflection–polarization pattern of the flat water surface under a clear sky at sunset. Owing to this technique and several fortunate circumstances, we could experimentally test and prove the validity of our earlier predictions. The prerequisites of this were the following.

(1) *An adequate technique to measure the polarization characteristics of the optical environment within a field of view of 180°*. "Point-source" polarimeters possess a very narrow (not wider than a few degrees) field of view (Azzam & Bashara, 1989; Collett, 1994). The fields of view of the different imaging polarimeters designed by Egan (1986), Prosch, Hennings, and Raschke (1983), Walraven (1981) and Wolff (1994), for instance, are limited to the field of view of the (video or photo) camera used being generally not larger than about 30°–40°. The entire celestial hemisphere and/or its water-surface-reflected image cannot be recorded with these polarimeters. Although the spherical convex mirror of the imaging polarimeter designed by North and Duggin (1997) possesses a field of view of almost 180°, reflection–polarization patterns of water surfaces cannot be recorded by it, because the camera of this equipment is set up on a huge tetrapod at a height of 6 m above the mirror (this nearly full-sky polarimeter is rather voluminous and cumbersome). Another method was developed by Liu and Voss (1997) and Voss and Liu (1997) for measuring full 180° field of view celestial polarization patterns. Neither of these methods is ideal for recording the mirror image of the sky reflected from a water surface. These sky polarimeters would not be practical for downward viewing polarimetry.

(2) *An appropriate method to record the mirror image of the sky in a field of view of 180°*. It is not simple to record the mirror image of the entire celestial hemisphere, that is, to record the entire water surface, because on the one hand a suitable propping up, or suspension of the camera is needed, which must not produce water ripples disturbing the reflection–polarization pattern of the water surface to be recorded. On the other hand, the mirror image of the propping or hanging up of the polarimeter should cover as small an area as possible on the mirror image of the sky.

(3) *A flat water surface as smooth as possible*. Due to the water ripples, the reflection–polarization patterns of a water surface change erratically in space and time. The theoretical calculations of Horváth (1995) and Schwind and Horváth (1993) were performed for an ideally flat water surface.

(4) *A body of water as dark as possible*. The light backscattered by the particles suspended in water and, furthermore, the light reflected from the bottom strongly influence the reflection–polarization pattern of the water surface. If the water body is dark enough due to light-absorbing particles suspended in the water and/or to the great depth of the water, then the effect of the small amount of light coming from the water is negligible with regard to the polarization in comparison with that of the light reflected from the water surface (Schwind, 1995). In this case, the polarization pattern of the water surface is determined predominantly by the surface-reflected skylight. In the theoretical calculations of Horváth (1995) and Schwind and Horváth (1993) it was assumed that light does not originate from the water.

(5) *A clear sky*. Haze and clouds strongly reduce the degree of polarization of skylight and can change its angle of polarization too. In the calculations of Horváth (1995) and Schwind and Horváth (1993) clear single-scattering Rayleigh skies were assumed.

These nontrivial prerequisites were fortunately all satisfied at 24:00 h (local summer time, UTC + 3) on 28 June 1999 on the banks of the river Oulu in the city of Oulu (Finland). Thus, we were able to record the reflection–polarization pattern of the flat water surface under a clear sky at sunset. In this work we present the measured reflection–polarization patterns and compare them with the theoretically calculated corresponding patterns.

2. Materials and methods

2.1. Measurement of the reflection–polarization pattern of the flat water surface by 180° field of view imaging polarimetry

The photographic records were taken by a Nikon F801 still camera equipped with a Nikon-Nikkor fisheye lens (*f* number: 2.8, focal length: 8 mm, angle of view: 180°)

including a built-in rotating disc mounted with three neutral grey linearly polarizing (HNP′B) filters with three different polarization axes (0°, 45° and 90° measured from the radius of the disc, Fig. 1A). Using Fujichrome Sensia II 100 ASA colour reversal film, the entire hemisphere of the optical environment (either the sky, or the water-surface-reflected sky) was photographed by this equipment through the three polarizing filters.

After an 8-bit (true colour) digitization (with a Hewlett Packard ScanJet 6100C) and evaluation of the three developed slides, the patterns of the degree and angle of polarization of the recorded hemisphere were determined with a personal computer and visualized as high-resolution colour-coded two-dimensional circular maps. The three colour-sensitive layers of the photoemulsion were known to exhibit maximal sensitivity at wavelengths $\lambda_{red} = 650$ nm, $\lambda_{green} = 550$ nm and $\lambda_{blue} = 450$ nm; the red, green and blue spectral ranges were obtained by using a digital image processing program provided with the scanner to digitally separate the colour channels in the digitized images. The computer evaluation of the three digitized colour photographs of a given scenery (that is, the reconstruction of the Stokes vector from the intensity measurements) was practically the same as that of the videopolarimetry described earlier by Horváth and Varjú (1997).

Our imaging polarimeter was calibrated. The reliability of the process of development of the colour reversal films was ensured in such a way that the films were developed always in the same professional Kodak Laboratory (Budapest) using the same automatically controlled method. In the evaluation of the recordings, that is, in the calculation of the brightness, degree and angle of polarization of skylight, the following characteristics of the recording and digitizing system were taken into consideration: (I) the measured Mueller matrix of the fisheye lens as a function of the angle of incidence with respect to the optical axis; (II) the measured angular distortion of the fisheye lens versus the angle of incidence; (III) the decrease of light intensity
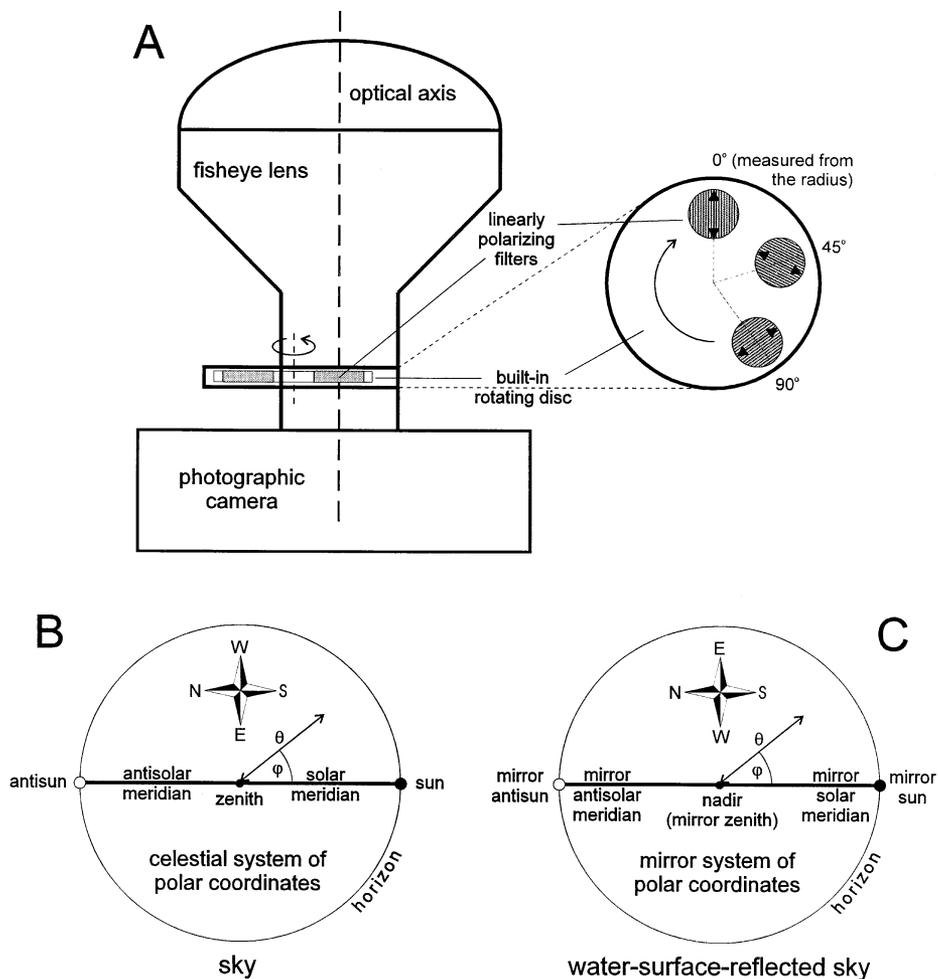

Fig. 1. Schematic representation of our 180° field of view rotating-analyzer imaging photopolarimeter (A), the celestial polar coordinate system (B) and the mirror system of polar coordinates fixed to the flat water surface (C) used in the calculations and visualization. The direction of the transmission axis of the polarizing filters is indicated by double-headed arrows in (A).

imaged on the photoemulsion because of the decrease of the effective aperture with increasing incident angle; (IV) the colour density curves of the colour reversal films (used as detectors) given by the producer; (V) the measured brightness and contrast transfer function of the scanner used for digitization of the colour slides of the sky. Characteristics (I)–(V) describe how the angular imaging, intensity, polarization, and spectral composition of the incident light are influenced by the optics and detector (photoemulsion) of the polarimeter and by the scanner (digitization). Although the responses of both photographic film and scanner were nonlinear, this was taken into account, because the transfer function between the digital brightness values and the density values of photoemulsion was measured, from which the incident light intensity was calculated, using the density–exposure characteristic curves of the film (given by the producer). Since further details of our instrument are not appropriate for this paper in this journal, a complete instrument analysis and description of our 180° field of view rotating-analyzer imaging photopolarimeter will be published elsewhere.

The measurement was performed at 24:00 h (local summer time, UTC+3) on 28 June 1999 on the shore of the river Oulu flowing through the city of Oulu (Finland) in westerly direction. At the time of the measurement (midnight) sunset occurred (Oulu is placed near the Arctic Circle) and the sky was clear, filling requirement (5) mentioned in the Introduction. Requirements (3) and (4) were also satisfied because we measured on that reach of the river where the water was dammed up at a power station. Due to the damming, the depth of the river was 10–15 m and consequently, its water was dark. In summer, the water of the river Oulu contains a large amount of dark brown light-absorbing suspended particles (tannin) of organic origin ("coloured dissolved organic material"), thus the water is primarily and naturally dark brown. The water surface was practically "mirror flat" because the water was quiet due to the damming and a period of calm.

Prerequisite (2) was satisfied in such a way that we recorded the mirror image of the blue sky from the end of a narrow jetty protruding into the calm and dark water perpendicularly to the shore. Standing on the end of the jetty, bending over the water surface through the railing of the jetty, and holding our polarimeter in hand, but fixed to a tripod in such a way that its optical axis was vertical, we recorded the reflection–polarization pattern of the water surface at a height of about 1 m from the water surface. By this recording method, we were able to minimize the area of the disturbing mirror image of the observer/recorder and the railing of the mole. Although the process of holding the camera out over the water was difficult, it was repeatable, because the camera was fixed to a tripod, which was fastened to the railing of the jetty and held by an assistant. Thus, any displacement of the camera could have been avoided between consecutive

exposures. Requirement (1) was satisfied by using 180° field of view imaging polarimetry. All images presented in this work were taken with the same exposure (1/60 s with aperture 8).

2.2. Calculations of the reflection–polarization pattern of the flat water surface

2.2.1. Calculation using single-scattering Rayleigh skylight pattern

The three-dimensional celestial hemisphere was represented in two dimensions by a polar-coordinate system, where the angular distance θ from the zenith and φ from the solar meridian are measured radially and tangentially, respectively (Fig. 1B). In this two-dimensional coordinate system, the zenith is at the origin and the horizon corresponds to the outermost circle. To display the reflection–polarization pattern of skylight visible over a flat water surface, a two-dimensional polar-coordinate system positioned parallel to the air–water interface was used (Fig. 1C). This system of coordinates is called the "mirror system," where the nadir ("mirror zenith"), "mirror sun," "mirror antisun," "mirror solar meridian" and "mirror antisolar meridian" correspond to the zenith, sun, antisun, solar and antisolar meridian of the celestial system, respectively. In the calculations, it was assumed that the air–water interface is flat, without ripples and the intensity of light arising from the reflection on the bottom and/or from scattering by particles suspended in water is negligible in comparison with the intensity of the water-surface-reflected light.

The theoretical polarization of the sky was described by the single-scattering Rayleigh model (Coulson, 1988). Apart from the Arago, Babinet and Brewster neutral points of skylight polarization, positioned at about ±25° to ±30°) from the solar and antisolar points along the solar and antisolar meridian of the firmament (Coulson, 1988; Horváth, Gál, Pomozi, & Wehner, 1998), the single-scattering Rayleigh model is a relatively good approximation of the celestial polarization pattern (Können, 1985).

Using Mueller calculations of light reflection without circular polarization component (Azzam & Bashara, 1989; Collett, 1994), the pattern of the degree and angle of polarization of Rayleigh skylight reflected from the flat water surface, furthermore the pattern of the reflectivity of the flat water surface were calculated as follows. The Stokes vector of the incident skylight is [Eq. (1)]:

$$\boldsymbol{S}^{\text{skylight}} = I^{\text{skylight}}(1, -\delta\cos2\alpha, \delta\sin2\alpha, 0), \qquad (1)$$

where I^{skylight} is the intensity, δ is the degree of polarization and α is the angle of polarization of skylight measured from the local meridian passing through the celestial point observed (that is, the direction of the local meridian was the reference direction for the Stokes vector).

The Mueller matrix of reflection of the flat air–water interface is [Eq. (2)]:

$$M^{refl} = \frac{1}{2} \left(\frac{\tan\Delta\theta}{\sin\theta_{sum}} \right)^2$$

$$\times \begin{bmatrix} \cos^2\Delta\theta + \cos^2\theta_{sum} & \cos^2\Delta\theta - \cos^2\theta_{sum} & 0 & 0 \\ \cos^2\Delta\theta - \cos^2\theta_{sum} & \cos^2\Delta\theta + \cos^2\theta_{sum} & 0 & 0 \\ 0 & 0 & -2\cos\Delta\theta\cos\theta_{sum} & 0 \\ 0 & 0 & 0 & -2\cos\Delta\theta\cos\theta_{sum} \end{bmatrix},$$

$$\Delta\theta = \theta_i - \theta_r, \quad \theta_{sum} = \theta_i + \theta_r, \tag{2}$$

where θ_i and θ_r are the angles of incidence and refraction, respectively. The Stokes vector of the reflected skylight is $S^{refl} = M^{refl}S^{skylight}$, from which the polarization parameters of the reflected skylight are the following [Eq. (3)]:

$$I_{reflected}^{skylight} = S_0^{refl}, \quad \delta = \sqrt{\frac{S_1^{refl\,2} + S_2^{refl\,2} + S_3^{refl\,2}}{S_0^{refl\,2}}}$$

$$\approx \sqrt{\frac{S_1^{refl\,2} + S_2^{refl\,2}}{S_0^{refl\,2}}}, \quad \text{because} \tag{3}$$

$$S_3^{refl} \approx 0; \quad \alpha = \frac{1}{2}\arctan\left[\frac{S_2^{refl}}{-S_1^{refl}} \right],$$

where S_n^{refl} ($n = 0, 1, 2, 3$) is the nth element of the Stokes vector. The reflectivity $R = I_{reflected}^{skylight}/I^{skylight}$ of the water surface was computed from pixel to pixel of the picture, where $I_{reflected}^{skylight}$ and $I^{skylight}$ are the intensity of the water-surface-reflected skylight (Fig. 3A) and the skylight (Fig. 2E), respectively.

2.2.2. Calculation using real skylight pattern

Using 180° field of view imaging polarimetry, we measured also the polarization pattern of the entire celestial hemisphere at 00:05 h (sunset) on 29 June 1999 on the shore of the river Oulu after the reflection–polarization pattern of the flat water surface had been measured with the same equipment. The measured maximum value of $\delta_{max} = 63\%$ of the degree of polarization of the skylight (at the zenith) was used for the single-scattering Rayleigh model. Using the Fresnel formulae (Mueller calculus; Guenther, 1990) and the computational method of Horváth (1995), the patterns of the degree and angle of polarization and the reflectivity of the flat water surface were calculated for the measured real skylight pattern. In these calculations a constant value of $n_{water} = 1.333$ was used for the refractive index of water.

3. Results

Fig. 2A and B shows the spatial distribution of the degree and angle of polarization of single-scattering Rayleigh skylight calculated for sunset ($\theta_s = 90°$, sun on the horizon). The angle of polarization of skylight is measured from the local meridian passing through the observed point of the celestial hemisphere. Fig. 2C–E shows the pattern of the degree of polarization, angle of polarization and intensity of skylight measured by 180° field of view imaging polarimetry in the green (550 nm) range of the spectrum at 00:05 h (sunset) on 29 June 1999 in Oulu.

Comparing Fig. 2A and C, we can establish that the single-scattering Rayleigh model describes relatively well the spatial distribution of the degree of polarization of skylight. There are, however, slight differences between the theoretical and measured patterns of the angle of polarization as can be seen if we compare Fig. 2B and D: (i) The ∞-shaped grey region is shorter in the measured pattern of the angle of polarization (Fig. 2D) than in the Rayleigh pattern (Fig. 2B). The Arago and Babinet neutral points of the skylight polarization are positioned at the left and right tips of this ∞-shaped region, respectively, where the positive polarization switches to negative polarization (Horváth et al., 1998). In the single-scattering Rayleigh model these neutral points coincide with the antisun and sun. (ii) The borderlines dividing the black and white regions are S-shaped in the real pattern of the angle of polarization (Fig. 2D) but straight in the Rayleigh pattern (Fig. 2B).

Fig. 3B–D represents the theoretical patterns of the degree and angle of polarization and reflectivity of the flat water surface calculated for the single-scattering Rayleigh skylight (Fig. 2A, B) with the use of the Fresnel formulae (Mueller calculus). Fig. 3E–G shows the same reflection–polarization patterns of the flat water surface computed for the measured skylight (Fig. 2C–E) with the use of the Fresnel formulae. The reflection–polarization patterns in Fig. 3E–G are semiempirical, because the "input" (incident skylight) was the real celestial polarization pattern measured by 180° field of view imaging polarimetry, while the "output" (reflected skylight) was calculated theoretically on the basis of the Fresnel formulae.

In the elongated checkered area (in the immediate vicinity of the setting sun) in Fig. 2C–E the film was overexposed resulting in an unpolarized region of the picture after computer evaluation. In this region of the picture, the unpolarized light has an undefined angle of polarization. In the future such overexposure can be eliminated by decreasing the time of exposure. Although then other regions of the image may be underexposed, the problem of losing polarization information in these underexposed regions can be partly solved by using a 12-bit or 16-bit digital camera providing an increased dynamic range compared to our present 8-bit configuration.

Fig. 3H–J shows the reflection–polarization patterns of the degree and angle of polarization and reflectivity of the flat water surface measured by 180° field of view imaging polarimetry in the green (550 nm) spectral range. Fig. 3A represents the corresponding mirror image of the sky reflected from the flat water surface in the green range of the spectrum. The triangular region on the right-hand side of
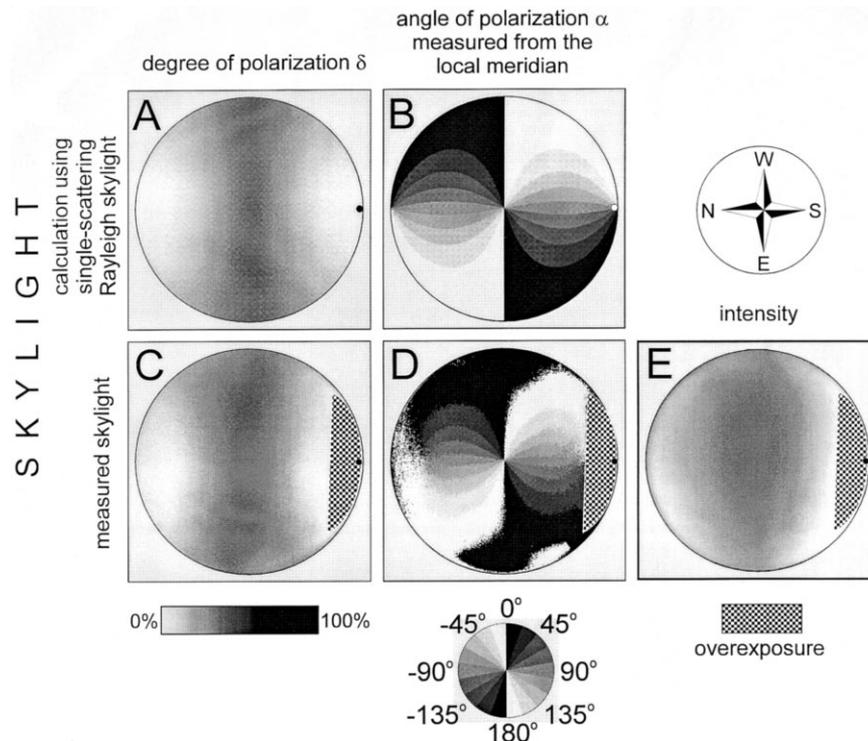
Fig. 2. (A, B) Spatial distribution of the degree δ and angle α of polarization of skylight calculated on the basis of the single-scattering Rayleigh theory for sunset ($\theta_s = 90°$, sun on the horizon). (C, D, E) Patterns of the degree of polarization, angle of polarization and intensity of skylight measured by 180° field of view imaging polarimetry in the green (550 nm) range of the spectrum at 00:05 h (sunset, local summer time, UTC + 3) on 29 June 1999 in Oulu. The checkered regions in patterns C–E are overexposed. The insets at the bottom show the grey tone coding of the different values of the degree and angle of polarization. The angle of polarization of skylight is measured from the local meridian passing through the observed point of the celestial hemisphere. The position of the sun is represented by black or white dots and the horizon is indicated by black circles.

these pictures is the railing at the end of the jetty from which the recording was taken. Although the mirror image of the railing screens out the mirror image of the sky in the vicinity of the setting sun, this does not matter because of the axial symmetry of the reflection–polarization pattern at sunset. The checkered narrow annular region in Fig. 3A, H–J was overexposed due to the large amount of light reflected from the water surface near the horizon. (The reflectivity of the flat water surface approximates 100% if the angle of reflection measured from the vertical nears 90°.) Similarly to Fig. 2C–E, this overexposure could be eliminated by decreasing the time of exposure, but then the central region of the picture would be underexposed.

In this work we present only the measurements in the green (550 nm) range of the spectrum. We measured these patterns also in the red (650 nm) and blue (450 nm) spectral ranges and obtained practically the same results. Thus, we omit presenting here the patterns measured in the red and blue ranges.

4. Discussion and conclusion

Comparing the theoretical, semiempirical and measured reflection–polarization patterns of the flat water surface

presented in Fig. 3B–D, E–G and H–J, we notice a remarkable resemblance between them. The reason for this close similarity is that the strong repolarization ability of the water surface overwhelms the slight differences between the polarization of the single-scattering Rayleigh and real sky-light. Apart from the overexposed regions and the mirror image of the railing of the jetty, the reason for the small, irrelevant differences between the measured (Fig. 3H–J) and predicted (Fig. 3E–G) reflection–polarization patterns may be that (i) the water surface was probably slightly undulating, and/or (ii) the optical axis of our polarimeter was perhaps not exactly vertical, and/or (iii) some light was scattered inside the water, then bounced back out; this reemitted radiation from the water was not taken into consideration in the prediction. At the periphery of the pictures in Fig. 3A, H–J the shore of the river Oulu is visible, which is the reason for the differences occurring at the periphery between the reflection–polarization patterns in Fig. 3B–D, E–G and H–J.

Analysing the fine details of the reflection–polarization patterns in Fig. 3 we can establish the following: The maximum (approximately 100%) degree of polarization of reflected skylight is located in a characteristic annular band, called the Brewster zone (from which the light is reflected with an angle of reflection of 53° called the Brewster angle),
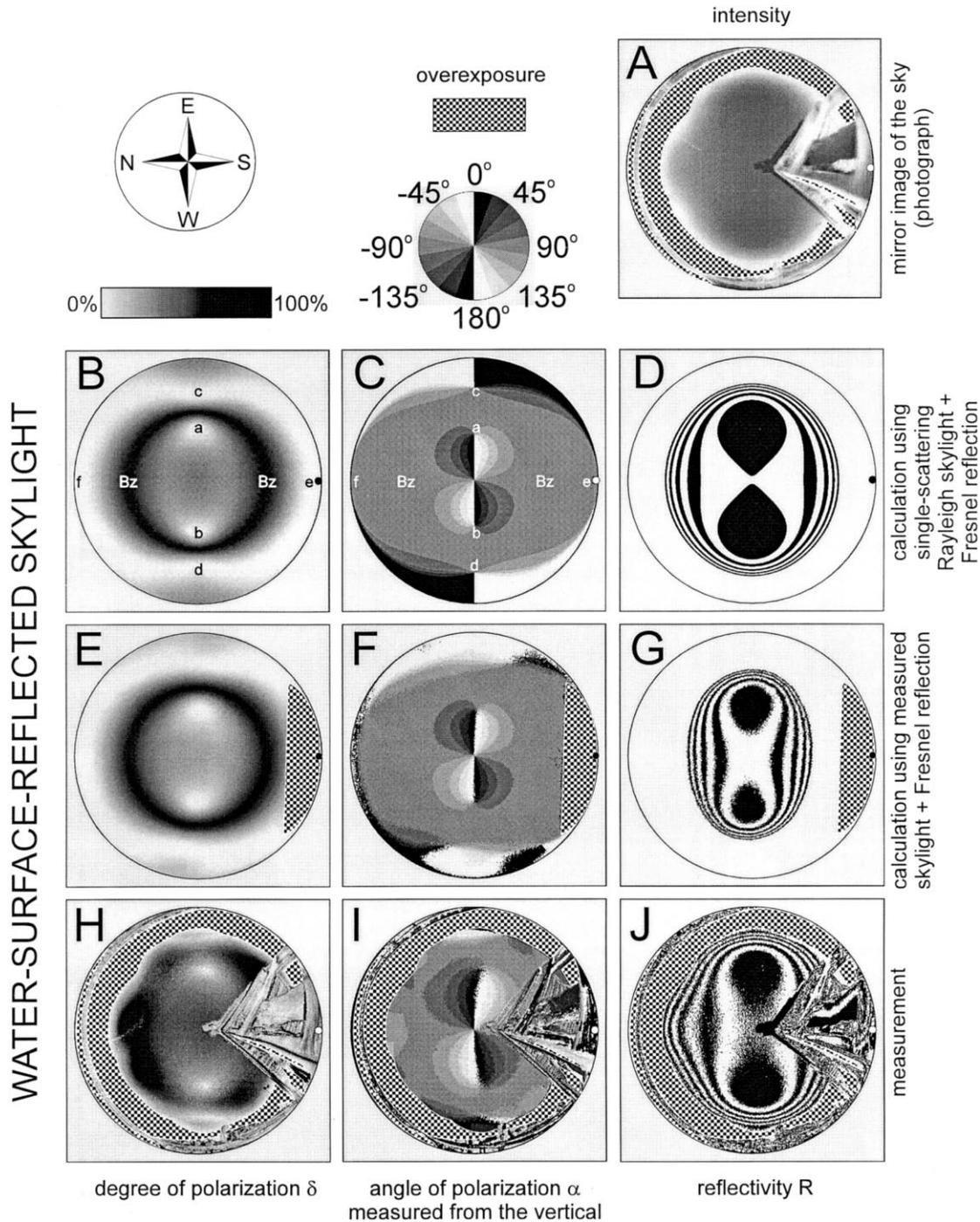
Fig. 3. (A) Intensity of skylight reflected from the flat water surface in the green (550 nm) range of the spectrum at 00:05 h (sunset, local summer time, UTC + 3) on 29 June 1999 in Oulu. (B, C, D) Theoretical patterns of the degree of polarization δ, angle of polarization α and reflectivity R of the flat water surface calculated for the single-scattering Rayleigh skylight (Fig. 2A, B) with the use of the Fresnel formulae (Mueller calculus). a, b, c, d, e, f: neutral points on the water surface; Bz: Brewster zone. (E, F, G) Reflection–polarization patterns of the flat water surface calculated for the measured real skylight pattern [in the green (550 nm) spectral range; Fig. 2C, D, E] with the use of the Fresnel formulae. (H, I, J) Reflection–polarization patterns of the flat water surface measured by 180° field of view imaging polarimetry in the green (550 nm) spectral range. The checkered regions in patterns A, E–G, and H–J are overexposed. The insets at the top show the grey tone coding of the different values of the degree and angle of polarization. The colour coding of the reflectivity values R is the following: The two central 8-shaped black patches in D, G, J represent R ≤ 2%. The concentric oval and annular, alternately black and white narrow zones around these patches represent R = 3%, 4%, ..., 9%, 10% towards the periphery. The outermost annular wide white (or checkered) zone represents R > 10%. The angle of polarization of light reflected from the water surface is measured from the vertical. The position of the mirror sun is represented by black or white dots and the horizon is indicated by black circles.

centred at a nadir angle of 53° at all azimuths around the point of observation (Fig. 3B, E, H). When the sun is on the horizon (sunset or sunrise) the Brewster zone with a strong horizontal polarization is maximally extended towards and away from the sun and becomes narrowest perpendicular to this direction.

At sunset (and sunrise) the flat water surface is mainly horizontally polarized (angle of polarization of the reflected light is $45° \leq \alpha \leq 135°$ with respect to the vertical) both in the direction of the sun and opposite to it, but apart from the horizontally polarized Brewster zone it is mainly vertically polarized ($0° \leq \alpha \leq 45°$ and $135° \leq \alpha \leq 180°$ with respect to the vertical) at right angles to the mirror solar meridian (Fig. 3C, F, I) just like the blue sky itself (Fig. 2B, D). At twilight the mainly vertically polarized region of the water surface (shaded with dark and bright grey) is 8-shaped within the Brewster zone and takes an extended bow shape outside the Brewster zone.

At twilight under a clear sky there are several neutral points on the water surface (Fig. 3B, E, H): Inside the Brewster zone (Bz) there exist two neutral points (a, b) positioned at about 45° from the nadir at right angles to the mirror solar meridian. There are two additional neutral points (c, d) outside the Brewster zone perpendicularly to the mirror solar meridian, and two further neutral points, the position of which coincides with the mirror sun (e) and the mirror antisun (f). These neutral points are the regions of the water surface where the horizontal polarization of reflected skylight switches to vertical.

The reflectivity pattern of the flat water surface has a quasi-cylindrical symmetry for reflectivity values larger than about 7%, i.e., for directions of observation larger than 65° from the vertical. The contour lines of equal reflectivity are elongated perpendicularly to the mirror solar meridian. The two central patches in Fig. 3D, G, J show those regions of the water surface where the reflectivity is not greater than 2%. These two dark patches can be seen on the water surface at 90° from the sun when it is near the horizon. The surface is clearly more transparent at these patches. The occurrence of these patches is the result of the fact that the reflectivity of the water surface is smaller for vertically polarized incident light than for horizontally polarized light (Horváth, 1995; Können, 1985).

The reflection–polarization patterns visible over the flat water surface under a clear sky at sunset (or sunrise) have characteristic gradients of the degree and angle of polarization and reflectivity. These different gradients are associated with the same regions of the water surface: where the reflectivity gradient is large, so too are the gradients for the degree and angle of polarization. This can be seen, for example, in the case of the characteristic 8-shaped pattern inside the Brewster zone in Fig. 3C, F, I. The tips of this 8-shaped pattern coincide with the two neutral points (a, b) of the pattern of the degree of polarization (Fig. 3B, E, H) and with the centre of the two dark patches of the reflectivity pattern (Fig. 3D, G, J).

The fact that the measured polarization pattern agreed so closely with that predicted by Horváth (1995) and Schwind and Horváth (1993) indicates that the simple single-scattering Rayleigh theory and Fresnel theory can accurately model the reflection of sky polarization at a flat air–water interface.

Finally, we would like to mention that the kind of 180° field of view imaging polarimetry designed by us may be useful not only in atmospheric optics, meteorology, or remote sensing, but also in biology for research on animals possessing polarization vision and using skylight polarization or water-surface-reflected polarized light for navigation, orientation and habitat selection. Our 180° field of view imaging polarimetry can help us understand important aspects of the visual behaviour of these animals.

Acknowledgements

References

Azzam, R. M. A., & Bashara, N. M. (1989). *Ellipsometry and polarized light*. Amsterdam: North-Holland.

Collett, E. (1994). *Polarized light. Fundamentals and applications*. New York: Marcel Dekker.

Coulson, K. L. (1988). *Polarization and intensity of light in the atmosphere*. Hampton, VA: A. Deepak Publishing.

Egan, W. G. (1986). Proposed design of an imaging spectropolarimeter/photometer for remote sensing of earth resources. *Optical Engineering*, *25*, 1155–1159.

Guenther, R. D. (1990). *Modern optics*. (Chapter 3: Reflection and Refraction, pp. 61-87) John Willey & Sons, Inc., New York.

Horváth, G. (1995). Reflection–polarization patterns at flat water surfaces and their relevance for insect polarization vision. *Journal of Theoretical Biology*, *175*, 27–37.

Horváth, G., Gál, J., Pomozi, I., & Wehner, R. (1998). Polarization portrait of the Arago point: video-polarimetric imaging of the neutral points of skylight polarization. *Naturwissenschaften*, *85*, 333–339.

Horváth, G., & Varjú, D. (1997). Polarization pattern of freshwater habitats recorded by video polarimetry in red, green and blue spectral ranges and its relevance for water detection by aquatic insects. *Journal of Experimental Biology*, *200*, 1155–1163.

Horváth, G., & Wehner, R. (1999). Skylight polarization as perceived by desert ants and measured by video polarimetry. *Journal of Comparative*

Physiology, A: Sensory, Neural, and Behavioral Physiology, *184*, 1–7 (Erratum 184, 347–349 (1999)).

Können, G. P. (1985). *Polarized light in nature*. Cambridge Univ. Press, Cambridge.

Liu, Y., & Voss, K. J. (1997). Polarized radiance distribution measurements of skylight: II. Experiment and data. *Applied Optics*, *36*, 8753–8764.

Mobley, C. D. (1994). *Light and water*. San Diego: Academic Press.

North, J. A., & Duggin, M. J. (1997). Stokes vector imaging of the polarized sky-dome. *Applied Optics*, *36*, 723–730.

Prosch, T., Hennings, D., & Raschke, E. (1983). Video polarimetry: a new imaging technique in atmospheric science. *Applied Optics*, *22*, 1360–1363.

Schwind, R. (1995). Spectral regions in which aquatic insects see reflected polarized light. *Journal of Comparative Physiology, A: Sensory, Neural, and Behavioral Physiology*, *177*, 439–448.

Schwind, R., & Horváth, G. (1993). Reflection–polarization pattern at water surfaces and correction of a common representation of the polarization pattern of the sky. *Naturwissenschaften*, *80*, 82–83.

Shaw, J. A. (1999). Degree of linear polarization in spectral radiances from water-viewing infrared polarimeters. *Applied Optics*, *38*, 3157–3165.

Voss, K. J., & Liu, Y. (1997). Polarized radiance distribution measurements of skylight: I. System description and characterization. *Applied Optics*, *36*, 6083–6094.

Walraven, R. L. (1981). Polarization imagery. *Optical Engineering*, *20*, 14–18.

Wolff, L. B. (1994). Polarization camera for computer vision with a beam splitter. *Journal of the Optical Society of America A: Optics, Image Science, and Vision*, *11*, 2935–2945.